Averaged Voronoi Polyhedron
in the Equiaxed Solidification Modelling

A.A. Burbelko[1*], J. Początek[1], W. Kapturkiewicz[1], and M. Wróbel[1]

[1]AGH University of Science and Technology, Krakow, Poland

For the modelling of the equiaxed grain growth controlled by diffusion the spherical *Elementary Micro-Diffusion Field* (EMDF) is usually used. Unfortunately, deviation of the idealized spherical grain geometry from the real one increases with a distance from nuclei. The proposed model of the equiaxed solidification, controlled by diffusion, assumes that EMDF has non-spherical shape as a result of random contacts between the grains growing around the individual nuclei. To determine the geometry and characteristics of the proposed EMDF, Kolmogorov's principle of the statistical theory of crystallization has been used. Modelling based on the non-spherical EMDF gives more accuracy of the solidification path prediction at the last stage of solidification. The results of simulation have been compared with experimental results obtained for near-peritectic Pb-Bi alloy.

Keywords: phase transformation modelling, equiaxed growth, elementary micro-diffusion field, ductile iron, averaged Voronoi polyhedron.

Introduction

Most advanced micro-models of the equiaxed solidification take into account the diffusion field in the vanishing liquid phase, as well as back diffusion in the grains of the solid phases. They are based on the spherical shape of the *Elementary Micro-Diffusion Field* (EMDF). Very often the subject of the investigations is a ductile iron (DI).[1-6] Due to the spherical symmetry of the nodular graphite in the DI the diffusion field of components was modelled as a 1D diffusion task. Models of such type are used also for the equiaxed peritectic solidification simulation.[7-11]

In the known numerical *Spherical Models* (SM) usually the idealized geometry of the EMDF is used. Spherically symmetrical cell of R_S radius was applied:

$$R_S = \sqrt[3]{\frac{3}{4\pi n}}$$

(1)

where n is the number of grains per unit volume, m[-3].

The above approximation has a satisfactory accuracy of the concentration profile prediction in the area placed not far from the grain nucleus but doesn't take into account the distortion of the peripheral area of the EMDF. Real shape of the grains is not spherical due to the grains impingements. Moreover, more than a third of the initial area remains outside the analysed space if the n grains of R_S radius were placed in the unit volume randomly and uniformly. This estimation is obtained on the base of the Kolmogorov statistical theory of solidification.[12] Bigger EMDF size was used in some models[8,13] to compensate lack of volume balance mentioned above. In this case prediction of the concentration profile becomes possible for the areas more remote from the grain centre. For the accounting of the grain overlapping effect in these models the Kolmogorov equation is used. Unfortunately these solutions have the serious shortcoming, because the question of mass balance of the solute elements remains unclear.

Equiaxed alloy microstructure obtained as a result of growth with a spherical symmetry may be approximated by a Voronoi tessellation. The scheme of the 2D tessellation for the image of ductile iron microstructure is shown in Fig. 1a. Domain of the one grain consists of the points closest to the grain nucleation centre rather than any other. Outer borders of the equiaxed grains are represented by straight segments perpendicular to the line connected the centres of the neighbouring grains in its middle point.

Two-dimensional Granular Model (GM) of solidification based on the 2D Voronoi tessellation has been developed by Vernède et al.[14,15] Phillion et al.[16] have also developed a semi-solid model based on similar granular structures. Solidification and micro-segregation in 2D GM were analysed in the triangular EMDF domains generated by two segments connecting the nucleation centre and corners of Voronoi cell (Fig. 1b). The geometrical approach like above can be easily extended to three dimensions for which the Voronoi tessellation will produce tetrahedral elements as a shape of EMDF[17]. Solidification model based on Voronoi diagrams was used also for the prediction of alloy's behaviour during solidification.[18-20]

The final grain structure and the shapes of the triangular/tetrahedral EMDF in these cases are the results of the preliminary Voronoi tessellation. In this 2D and 3D elementary cells the one-dimension micro-diffusion tasks were

---

solved individually for the every pair of symmetric cells. One-dimensional diffusion flow is directed from the grain nucleation centre to the outer border of the Voronoi polygons or polyhedra.
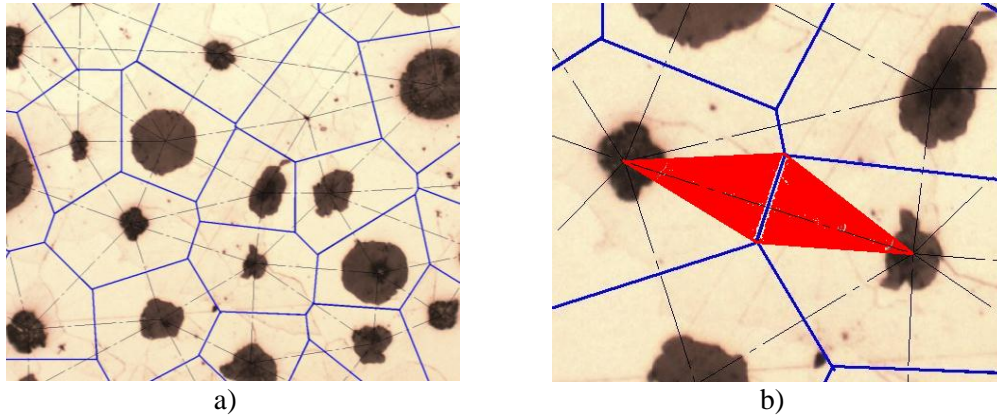

a)   b)

Fig.1: Scheme of the Voronoi tessellation of the 2D microstructure of the DI (a) and fragment of the left picture with the shape of the two symmetry diffusion cells in the adjacent Voronoi polygons (b).

Description of the Mathematical Model

In the SM as well as in GM the one-dimension solute distribution $C(x,\tau)$ was obtained by numerical solution of the diffusion equation:

$$\frac{\partial C(x,\tau)}{\partial \tau} = \text{div}[D \,\text{grad}\, C(x,\tau)] \tag{2}$$

where: D is the solute diffusion coefficient, $m^2 s^{-1}$; x is the distance from the EMDF centre, m; τ is time, s.

The equation (2) is solved by numerical computing in the time-varying domain of every phase with proper equilibrium solute concentration as the border conditions. Velocity of the mobile interface migration between the growing (α) and vanishing (β) phases is calculated on the base of mass conservation condition:

$$u_{\alpha/\beta}\left(\rho_\alpha C_\alpha - \rho_\beta C_\beta\right) = D_\alpha \rho_\alpha \left.\frac{\partial C_\alpha}{\partial r}\right|_\alpha - D_\beta \rho_\beta \left.\frac{\partial C_\beta}{\partial r}\right|_\beta \tag{3}$$

where: ρ is the phase density, $kg \cdot m^{-3}$; u is the velocity of interface of α-phase migration into the direction of the β-phase, $m \cdot s^{-1}$; lower indices denote the proper phase. Proper left-hand or right-hand derivative must be used for both phases.

In the derivation of the difference equations used for the numerical solution of the equation (2) the shape of the solution domain must be taken into account. The schemes of the control volumes (CV) tracing in the EMDFs for SM and GM are presented in Fig. 2a and 2b for the elementary balance calculation. Adjacent CVs cover entire volume of the EMDF.

In this paper the EMDF with the geometry of Averaged Voronoi Polyhedron (AVP) was used.[21-23] Example scheme of the CV location in the particular Voronoi polygon is shown in Fig. 2c. In the domain of every CV the uniform solute concentration is assumed. Diffusion flux of solute crosses the inner (F_i) and outer (F_{i+1}) borders of this CV only in the radial direction. All external boundaries of the Voronoi diffusion cells are assumed as adiabatic (like in the GM). In the SM adiabatic border condition is used only at the outer border of the EMDF. Differences between the GM and AVP scheme of the EMDF are as follows. In the GM every Voronoi cell volume is divided into the sectors: one EMDF consists from two symmetric cells placed in the adjacent polyhedron (see Fig. 1b). Number of the sectors is equal to the number of neighbour Voronoi polygons/polyhedra. All inner walls between the sectors are adiabatic as well as the outer borders of the Voronoi polygon / polyhedron (Fig. 2b). Parameters of CV in the AVP are calculated as averaged values like in the SM solution. These parameters in the AVP were determined for the set of Voronoi polyhedra. In the GM the individual positions of the phase border and transformed volume fractions are obtained by modelling for every EMDF. Model, based on the AVP, gives the mean values of interface position and the transformed volume for all grains growing in the micro-volume with a similar cooling path (like SM).

According to Kolmogorov[12], in the case of an instantaneous nucleation of the n grains in a unit volume and their spherical growth at the same (not necessarily constant) speed, the average volume of the material of one grain at the maximum distance r from the nucleation sites can be determined by the following equation:

$$V(r) = n^{-1}\left(1 - \exp\left(-\frac{4}{3}\pi n r^3\right)\right) \tag{4}$$

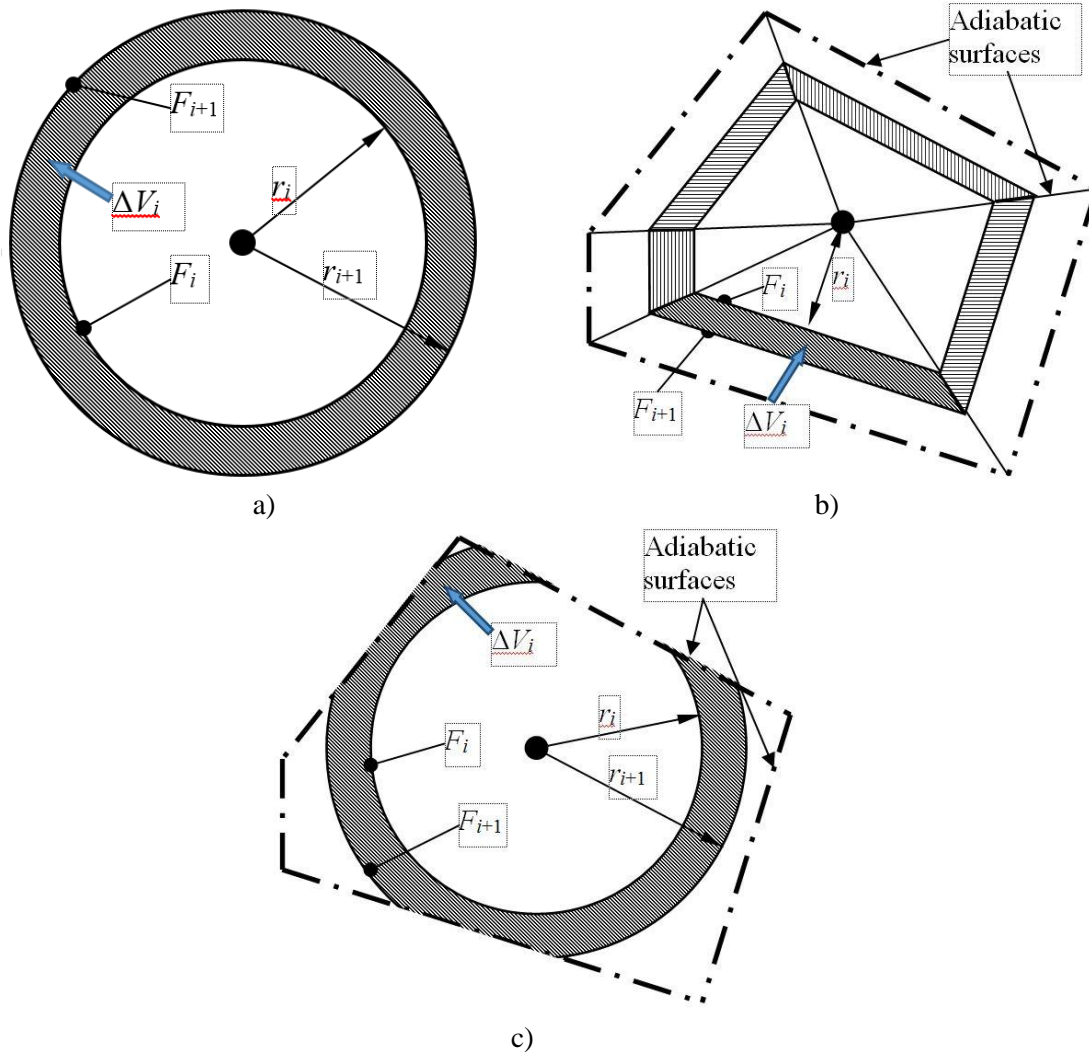where: n is a volumetric grain density, m^{-3}; r is a distance from grain centre, m.

Fig.2: The schemes of the solution domain regionalisation in the case of control volume solution method for different EMDF geometry: SM (a), GM (b), and Averaged Voronoi Polyhedron (c); ΔV_i is the volume of the control element; F_i, F_{i+1} are the surfaces of the inner and outer interfaces of the control element; r_i, r_{i+1} are the positions of the inner and outer interfaces in the EMDF.

For the simplification of the used notation the following E(n,r) function is introduced:

$$E(n,r) = \exp\left(-\frac{4}{3}\pi n r^3\right) \tag{5}$$

Main advantage of the AVP scheme over the SM one is the proper choice of the EMDF size. Maximum size of the particular Voronoi Polyhedron is infinite. Shape of its body, number of faces, edges and vertices are the random values. However from equation (4) it follows that for the random set of the Voronoi polyhedra the averaged volume fraction belonging to the polyhedra and being at the distance less then r from their centres is equal to:[21]

$$\varepsilon = E(n,r) \tag{6}$$

Finishing radius of the EMDF R_{EMDF} in this case can be estimated after all grains have nucleated, on the base of grain number and desired accuracy of volume calculation ε:

$$R_{EMDF} \geq \sqrt[3]{-\frac{3\ln\varepsilon}{4\pi n}} \tag{7}$$

Size of the CV showed in Fig. 2c can be computed as follow:

$$\Delta V_i = n^{-1}\left[E(n,r_i) - E(n,r_{i+1})\right] \tag{8}$$

Inner surface of this CV can be calculated by derivation of equation (4) with respect to r:

$$F_i = 4\pi r_i^2 E(n,r_i) \tag{9}$$

The set of the difference equations for elementary balance method can be derived on the base of equations (5), (8), and (9).

Calculation of the volumetric rate of the $\alpha \rightarrow \beta$ precipitation is available on the base of equation (9):

$$v_{\alpha/\beta} = 4\pi n r_{\alpha/\beta}^2 u_{\alpha/\beta} E\left(n, r_{\alpha/\beta}\right), \ \mathrm{s}^{-1} \tag{10}$$

Simulation Conditions

Modelling has been performed for two binary model alloys: eutectic Fe-C and hyperperitectic Pb-Bi (32 wt.%Bi). Diffusion coefficients used in the calculation are shown in the Table 1. Number of the eutectic cells equal to $1.96 \cdot 10^{13}$ m^{-3} was imposed for Fe-C alloy and for Pb-Bi system number of peritectic cells of $1.0 \cdot 10^{12}$ m^{-3} was chosen.

For Fe-C alloy the equilibrium concentrations for equation (3) have been computed for the given temperature by means of CALPHAD method,[24] using Thermo-Calc Software with Thermodynamic Calculation Interface (TQ-Interface). For the Pb-Bi alloy the values of equilibrium concentration were calculated by linear relations shown in Table 1. Equation parameters presented in this table are obtained on the base of binary Pb-Bi equilibrium thermodynamic system calculated by Thermo-Calc. Diffusion coefficients of the solutes used in the modelling are shown in Table 2.

Table 1: Equilibrium temperature of the Pb-Bi system.

Equilibrium Phases		Equilibrium Bi concentration, wt.%	
I	II	I phase	II phase
Liquid	Pb (FCC)	$0.85969 - 2.6290 \cdot 10^{-3} \cdot T$	$0.53132 - 1.6248 \cdot 10^{-3} \cdot T$
Liquid	ε-Pb (HCP)	$0.93469 - 3.0375 \cdot 10^{-3} \cdot T$	$0.71370 - 2.2696 \cdot 10^{-3} \cdot T$
Pb (FCC)	ε-Pb (HCP)	$0.16933 - 3.4678 \cdot 10^{-4} \cdot T$	$0.24491 + 2.8373 \cdot 10^{-4} \cdot T$

Table 2: Diffusion coefficients.

Element	Phase	Diffusion coefficient, m^{2}s^{-1}	Source
C	Liquid Fe-C (Liq)	$1.25 \cdot 10^{-9}$	[25]
C	Austenite (FCC)	$1.5 \cdot 10^{-10}$	[25]
Bi	Liquid Pb-Bi (Liq)	$1.3 \cdot 10^{-9}$	[26]
Bi	Pb (FCC)	$1.0 \cdot 10^{-14}$	[8]
Bi	ε-Pb (HCP)	$2.0 \cdot 10^{-14}$	

Modelling Results

Decreasing intensity of external cooling was assumed for Fe-C alloy solidification:

$$Q = -5.082 \cdot c \cdot \exp\left(-5.307 \cdot 10^3 \cdot \tau\right), \ \mathrm{W \cdot m}^{-3} \tag{11}$$

where: c is a volumetric specific heat of alloy, J·m^{-3}K; τ is time, s. Above heat extraction rate is typical for DI casting with 9 mm thick wall, made in the greensand mould. Results of the micro-modelling are presented in Fig. 3 and 4. Cooling curves presented in Fig. 3 were calculated with a numerical solution of the differential heat balance equation:

$$c \frac{\partial T}{\partial \tau} = Q - \sum_j \left(v_j H_j\right) \tag{12}$$

were H is the enthalpy of the phase transformation (see Table 3). Summation in the equation (12) is performed for all phase transformations j.

Table 3: Enthalpy of the precipitations.

Precipitation	Transformation Enthalpy, J·m^{-3}	Source
Austenite from Liquid	$1971.0 \cdot 10^6$	[27]
Graphite from Austenite	$0.88 \cdot 10^6$	

Calculations were performed by SM and AVP methods with mesh step 1 μm. For SM radius of the EMDF was obtained by equation (1) as 23 μm and for AVP by equation (7) as 44 μm ($\varepsilon = 0.001$). At the beginning of the eutectic

solidification the differences between temperature-time curves produced by SM and AVP method of simulation is very small. Calculated transformation rate in the SM is slightly higher than in the AVP. Accumulation of these differences over a period of the whole solidification time (88 s) results with the 5 K higher temperature of an alloy in the SM method. At that instant, the untransformed liquid fraction in the AVP model is near to the 2.5 vol.%. In the AVP modelling solidification ends near the 5 s later. Shape of the simulated cooling curve at the instant of the transformation completion obtained with the AVP confirms model assumptions in terms of quality.

Simulated changes of the graphite nodules mean size is presented in Fig. 4a as well as the position of the solid-liquid interface. Values of the interface migration velocity are shown in Fig. 4b. As it follows from these diagrams, the SM and AVP models give the similar results for the domain placed near the nodule centre, at distance shorter the half of the EMDF radius calculated for SM using equation (1). This distance is indicated in Fig. 4a by a grey line. Size of the graphite spheres and velocity of the growth are very similar in the both models. Differences between austenite envelope radii become meaningful after 20 s of solidification. Acceleration of the solid-liquid interface predicted in the AVP model at the last stage of solidification is a well-known fact.
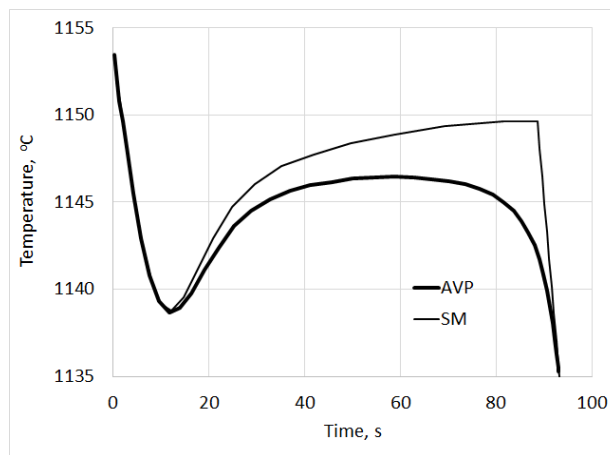

Fig.3: Calculated cooling curves obtained for eutectic Fe-C alloy with the SM and AVP models.
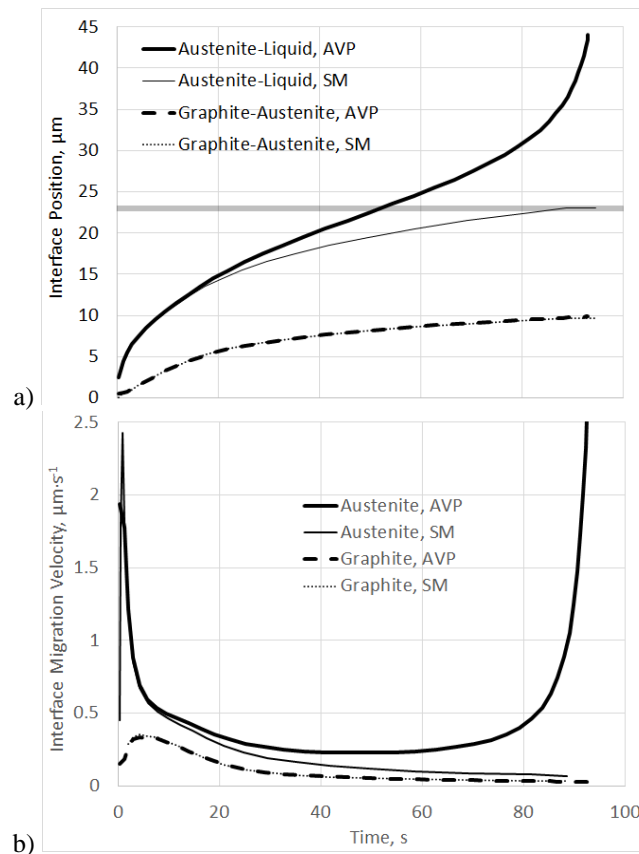

Fig.4: Changes of the interface position (a) and interface migration velocity (b) obtained in the modelling for eutectic Fe-C alloy with the SM and AVP models.

Hyper-peritectic Pb-Bi alloy has a similar shape of the EMDF scheme to eutectic DI. This alloy was used for the verification of the model correctness because of relatively simplicity to obtain the experimental results in comparison with Fe-C alloys. Modelling of the binary hyper-peritectic Pb – 32 wt.% Bi alloy solidification has been performed for the slow cooling of the sample with a furnace (cooling rate -0.011 K/s). Changes of the solid-liquid interface position for primary Pb solidification are shown if Fig. 5a together with the changes of the outer and inner interfaces positions of the peritectic ε-Pb layer in the contacts with the dissolved primary Pb and vanishing liquid phase. Changes of the phase volume fractions are presented in Fig. 5b. Modelling was performed by AVP methods with mesh step 1 μm. Radius of the EMDF was estimated by equation (7) as 188 μm ($\varepsilon = 0.001$).
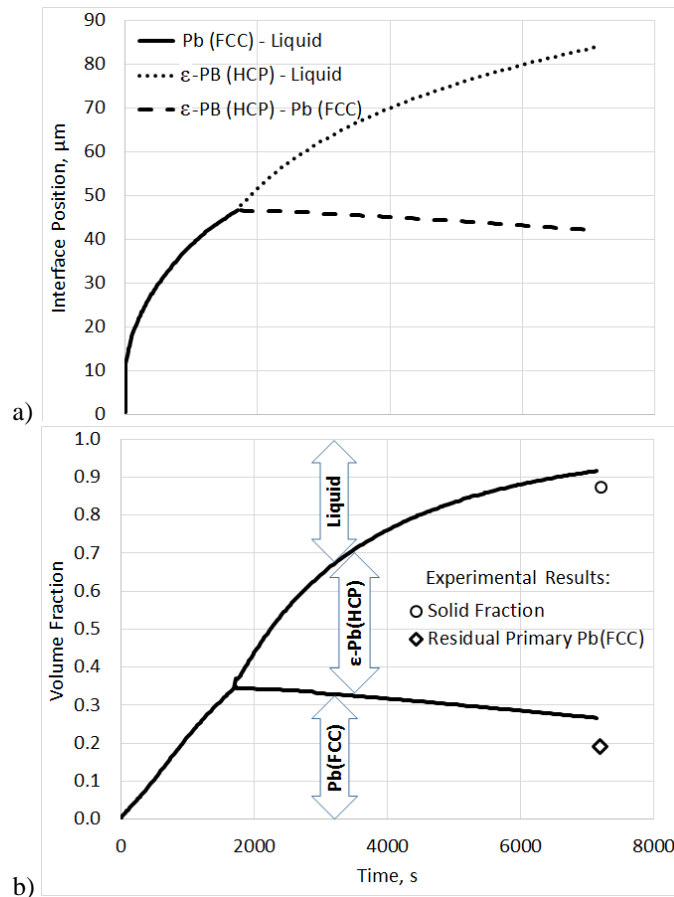

Fig.5: Changes of the interfaces positions (a) and volume fractions of the phases (b).

After cooling 5 K below the temperature of the eutectic equilibrium (120°C) the sample has been quenched in the water. Microstructure of the sample is presented in Fig. 6.
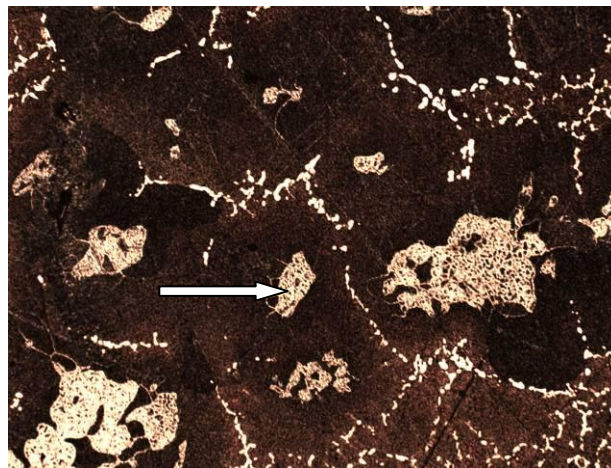

Fig.6: Microstructure of the analysed Pb-32%wt. Bi alloy, 200x.

Quantitative stereological analysis was performed for this sample. Random set of the 100 images obtained with magnification 1000x were analysed by manual point count method with using of the regular grid 11x11 points. Volume fraction of the residual primary Pb(FCC) measured by set of the 12100 points is equal to 19,15%. Measured volume fraction of the eutectic Bi is equal to 2.53%.

Chemical composition of the analysed alloy is shown in the binary Pb-Bi thermodynamic diagram in Fig. 7 by the grey vertical line. According to this diagram, in the quenching temperature this alloy has the single-phase ε-Pb structure. As it follow from Fig. 6, residual primary Pb(FCC) is observed in the sample structure (white arrow). Predicted volume fraction of this phase is in the accordance with results of quantitative metallography. Chains of the white Bi inclusion on the grain boundaries denote the eutectic composition of the liquid phase at the last stage of the sample solidification. This fact confirms the modelling results shown in Fig. 5b. On the base of the measured volume fraction of eutectic Bi, the residual volume fraction of liquid phase that solidify as the ε-Pb–Bi eutectic in the temperature of the eutectic equilibrium is estimated to be nearly 12%.
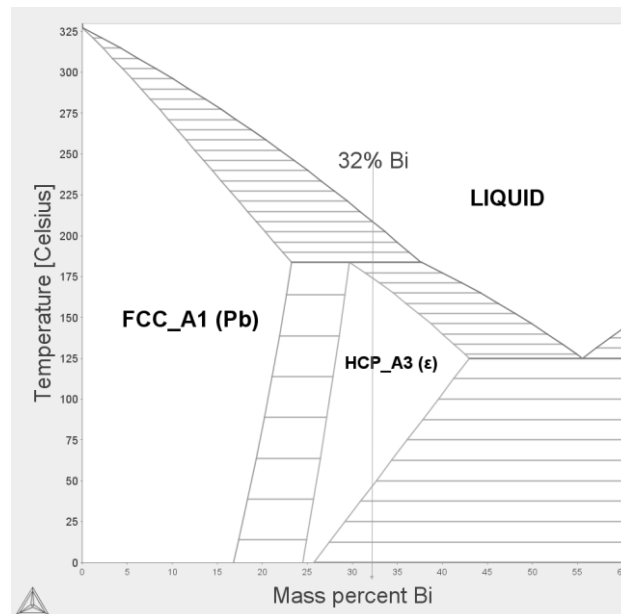

Fig.7: Fragment of the binary thermodynamic diagram Pb-Bi calculated by Thermo-Calc Software.

Discussion

Comparison of the simulation results and experimental one says about the qualitative confirmation of the AVP model rightness. It is shown that AVP model gives the better precision of the simulation for the equiaxed grain growth than SM at the final stages of the solidification. This is the result of the accounting of the actual surface area of contact between the growing solid and vanishing liquid placed in the intercrystalline space.

It is known fact that at the beginning stage the solidification of the globular graphite and austenite dendrites is not coupled: grains of both phases grow directly from liquid without common contacts. [28] Moreover, the solidification of some off-eutectic austenite is observed even in the hyper-eutectic alloys. [29] Due to this solidification mechanism the shape of the EMDF is more complicated.

The described above phenomenon was taking into account in the known models based on the SM. [5,6] To take into account the impingement of the spherical eutectic grains at the last stage of the solidification, so-called Kolmogorow-Avrami-Johanson-Mehl correction is used in these models. This is not fully accurate. Better mapping of the initial uncoupled graphite and austenite nucleation and growth as well as the transition to the stage of the coupled growth (in the eutectic, hypo- and hypereutectic alloys) gives the cellular automata technique. [30,31]

The presented version of the AVP model has a limitation and takes into account equiaxed growth only (for single primary phase as well as for few layers of solid phases). Taking into account the growth of the off-eutectic grains will be a subject of further work of the authors.

Conclusions

1. The Averaged Voronoi Polyhedron geometry for the EMDF description gets the averaged representation of the real shapes of the equiaxed grains better in comparison to known SM. Parameters of the AVP have been used for determining of EMDF in the micromodelling of the equiaxed stage of the primary, single-phase solidification (Pb in Pb-Bi), coupled stage of the eutectic solidification in the DI and peritectic solidification in the hyperperitectic Pb-Bi alloy.

2. AVP-based micromodelling gives better representation of the last stage of the equiaxed grain solidification then model with an ideal spherical shape of the EMDF because proposed characteristics of the AVP takes into account random nature of the impingements of the adjacent grains. In the DI presented version of the model doesn't take into account the possibility of the off-eutectic austenite dendrite solidification.
3. Results of the quantitative metallography for the Pb-32 wt.%Bi alloy confirm the correctness of the AVP model used for the modelling of the alloy solidification.

References

1. D. M. Stefanescu, A. Catalina, X. Guo, L. Chuzhoy, M. A. Pershing and G. L. Biltgen: Modeling of Casting, Welding and Advanced Solidification Process – VIII, The Minerals, Metals & Materials Society, Warrendale, PA, 1998, 455.
2. S. M. Yoo, A. Ludwig and P. R. Sahm: Solidification Processing, Renmor House, Univ. of Sheffield, Sheffield, 1997, 494.
3. S. Chang, D. Shangguan and D. M. Stefanescu: *Metall. Trans. A*, 1992, 23A, 1333-1346.
4. M. I. Onsoien, O. Grong, O. Gundersen and T. Skaland: *Metall. Mater. Trans. A*, 1999, 30A, 1053-68.
5. G. Lesoult, M. Castro and J. Lacaze: *Acta Mater.*, 1998, 46, 983-995.
6. J. Lacaze, M. Castro and G. Lesoult: *Acta Mater.*, 1998, 46, 997-1010.
7. A. Das, I. Manna and S.K. Pabi: *Scripta Mat.*, 1997, 36, 867-873.
8. A. Das, I. Manna and S.K. Pabi: *Acta Mater.*, 1999, 47, 1379-1388.
9. K. Matsuura, H. Maruyama, Y. Itoh, M. Kudoh and K. Ishii: *ISIJ Int.*, 1995, 35, 183-187.
10. M. El-Bealy and H. Fredriksson: *Met. and Mat. Trans. B.*, 1996, 27B, 999-1014.
11. E.P. Kalinushkin, E. Fras, W. Kapturkiewicz, A.A. Burbelko and J. Sitalo: *Mat. Sci. Forum*, 2000, 329-330, 185-190.
12. A.N. Kolmogorov: *Bull. Acad. Sci. USSR*, 1937, 3, 355-359 (in Russian).
13. E. Fraś, W. Kapturkiewicz and A.A. Burbelko: *Advanced Mat. Res.*, 1997, 4-5, 499-504.
14. S. Vernède, P. Jarry and M. Rappaz: *Acta Mater.*, 2006, 54, 4023-4034.
15. S. Vernède and M. Rappaz: *Acta Mater.*, 2007, 55, 1703-1710.
16. A.B. Phillion, S.L. Cockcroft and P.D. Lee: *Acta Mater.*, 2008, 56, 4328-4338.
17. S. Vernède and M. Rappaz: *Philosophical Magazine*, 2006, 86, 3779–3794.
18. A.B. Phillion, J.-L. Desbiolles and M. Rappaz: Modeling of Casting, Welding, and Advanced Solidification Processes – XII, TMS, 2009, 353-360.
19. S. Vernède, J.A. Dantzig and M. Rappaz: *Acta Materialia*, 2009, 57, 1554-1569.
20. A. B. Phillion, S. Vernède, M. Rappaz, S.L. Cockcroft and P. D. Lee: *Int. J. Cast Metals Research*, 2009, 22, 240-243.
21. A. Burbelko, J. Początek, D. Gurgul and M. Wróbel: *Steel Research Int.*, 2014, 6, 1010-1017.
22. A. Burbelko and J. Początek: The TMS 2013 Annual Meeting Supplemental Proceedings. TMS (The Minerals, Metals & Materials Society), John Wiley & Sons, Inc., 2013, p. 523-530.
23. A.A. Burbelko, J. Początek and M. Królikowski: *Arch. of Foundry Eng.*, 2012, 13, Iss. 1, 134-140.
24. H.L. Lukas, S.G. Fries and B. Sundman: 'Computational Thermodynamics: The Calphad Method', 2007, University Press, Cambridge.
25. P. Magnin, J.T. Mason and R. Trivedi: *Acta Met. Mat.*, 1991, 39, 469-480.
26. S. Liu and R. Trivedi: *Met. Mater. Trans. A*, 2006, 37A, 3293–3304.
27. I.K. Kikoin (Ed.): 'Tables of the physical parameters', 1976, Moscow, Atomizdat (In Russian).
28. H. Fredriksson, J. Stjerndahl and J. Tinoco: *Mat. Sci. Eng. A*, 2005, 413-14, 363-372.
29. M. Hecht and J.C. Margerie: *Memoires Scientifics De La Revue De Metallurgie*, 1971, 68, 325.
30. A. Burbelko, E. Fraś, D. Gurgul, W. Kapturkiewicz and J. Sikora: *Key Eng. Mater.*, 2011, 457, 330-336.
31. A.A. Burbelko, D. Gurgul, W. Kapturkiewicz and E. Guzik: *Mat. Sci. Forum*, 2014, 790-791, 140-145.

Acknowledgement